Hindawi Publishing Corporation
Advances in Astronomy
Volume 2010, Article ID 428943, 8 pages
doi:10.1155/2010/428943

Research Article

Detection of GRBs and OTs by All-Sky Optical and SID Monitors

R. Hudec,[1,2] M. Spurny,[3] M. Krizek,[4] P. Pata,[2] R. Slosiar,[5] M. Rerabek,[2] and M. Klima[2]

[1] *Astronomical Institute, Academy of Sciences of the Czech Republic, 251 65 Ondrejov, Czech Republic*
[2] *Faculty of Electrical Engineering, Czech Technical University in Prague, Technicka 2, 166 27 Prague 6, Czech Republic*
[3] *Karlovy Vary Observatory, K Letisti 144, 360 01 Karlovy Vary, Czech Republic*
[4] *Charles University, Astronomical Institute, 180 00 Prague, Czech Republic*
[5] *Partizanske Observatory, 958 04 Partizanske, Slovakia*

Correspondence should be addressed to R. Hudec, rhudec@asu.cas.cz

Received 13 June 2009; Accepted 15 November 2009

Academic Editor: Taro Kotani

We report on two alternative simple methods to detect counterparts of cosmic gamma-ray bursts (GRBs) and optical transients (OTs). We report on the development and tests of an alternative optical all-sky monitor recently tested at the Karlovy Vary Observatory. The monitor is based on a Peleng 8 mm fish-eye lens (1 : 3,5–1 : 16) and CANON EOS 350D digital CCD camera. This type of monitor represents a low-cost device suitable for easy replication and still able to detect brighter optical transients simultaneously to GRB triggers. Such OTs have been observed for some of the GRBs such as GRB990123, GRB060117, or recently GRB080319 indicating that some fraction of GRBs can generate optical transient emission accessible by simple small aperture instrumentation as described here. These efforts are accompanied by development of dedicated programmes to access and to evaluate all-sky images; these efforts will be also briefly described. The All-Sky Monitor is a space variant optical system and its point spread function (PSF) has not uniform shape in the field of view. The processing and measuring of image data is complicated, and sophisticated deconvolution algorithms are used for image restoration. The second method is the GRB detection based on their ionospheric response.

1. Bright Prompt Optical Emission of GRBs

The fast response is required to investigate the optical prompt emission of GRBs. However, even the fastest optical follow-up telescopes cannot access the times close or identical to times of GRBs, and the time domain before GRB remains completely hidden. These time domains can be accessed only by optical wide-field monitors (as the position of the GRB is unpredictable). The all-sky monitors offer the best sky coverage. An alternative approach is to monitor the FOVs of recent GRB satellites with optical WF cameras. Some of the all-sky monitors operated on daily basis are based on the use of photographic emulsion (allowing long exposures and fine spatial resolution of few microns). However, the photographic emulsion is not very sensitive to short optical flares and has some additional disadvantages. The alternative digital all-sky monitoring is provided by the CONCAM system. However, the limiting magnitudes are not very deep, so one can hardly expect that such system will be able to detect optical transients (OTs) of GRBs. The brightest OTs related to GRBs observed so far were observed at magnitudes 6–10 (e.g., GRB990123, GRB060117, GRB080319) [1, 2]. For GRB060117, the optical transient was followed due to technical reasons from 2 minutes after the GRB trigger and already declining, so one can deduce that the peak brightness probably exceeded magnitude 8 [3]. We hence need monitors able to detect short OTs with duration of about 1 minute and fainter than magnitude 8. Some optical all-sky monitors are in operation already such as the EN photographic network managed by the Ondrejov Observatory (Figures 5, 6, and 7) and CCD-based sky monitor was tested at the Sonneberg Observatory (Figure 4).

2. The Optical All-Sky Monitor

We report on an alternative low cost all-sky monitor. The used instrumentation is simple and low-cost. The camera

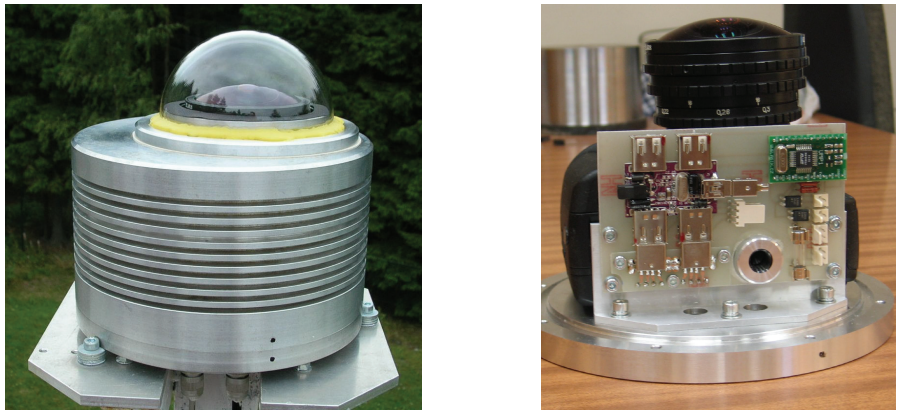

(a) (b)

Figure 1: The assembled all-sky camera in observing conditions (a) and the camera with control electronic board (b).

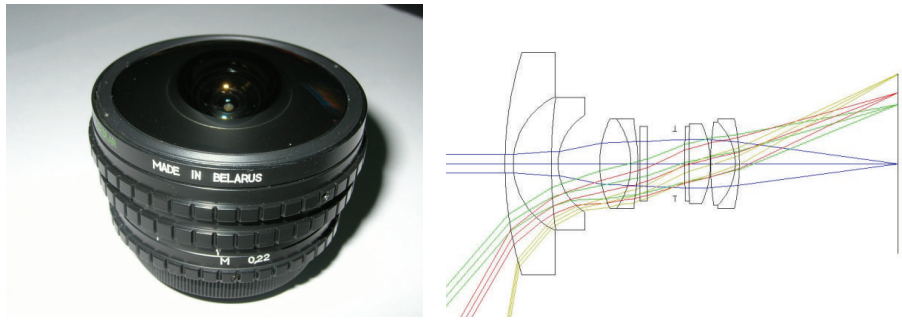

(a) (b)

Figure 2: The picture and the schema of the used Peleng fish-eye lens. It should be noted that the lens consist of 10 glass elements. Although no detailed measurements about spectral efficiency of the lens, by analogy with similar lenses, one can expect that there will be no or very little response below 400 nm.

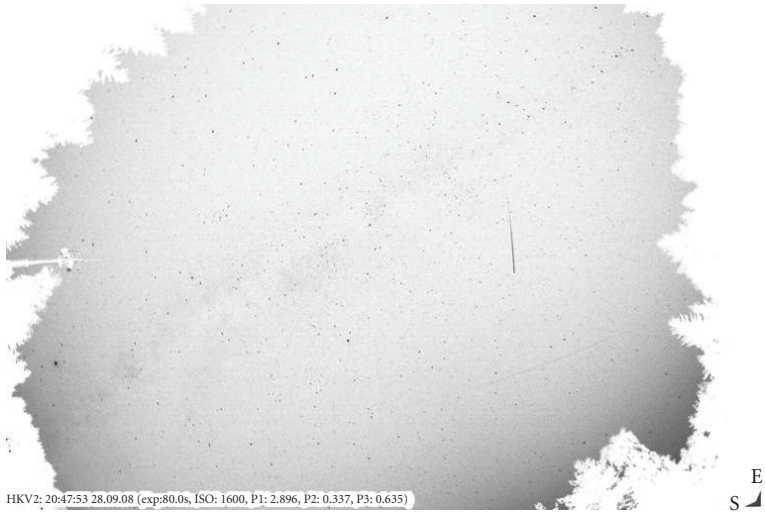

Figure 3: An example of raw nonguided image taken by the camera illustrated in Figure 1, exposure time 80 seconds (converted to negative).

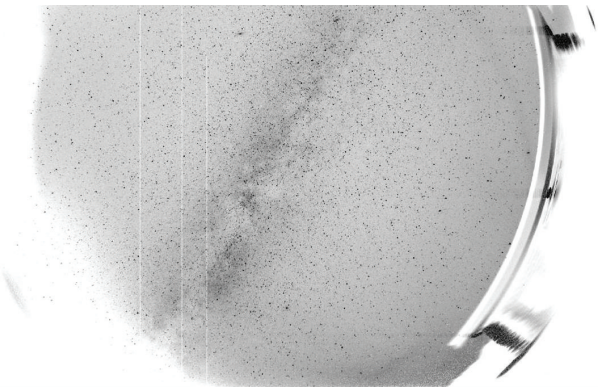

Figure 4: Sonneberg Observatory All-Sky 7 k × 4 k CCD camera, 10 minutes exposure, 4 × 4 binning (converted to negative).

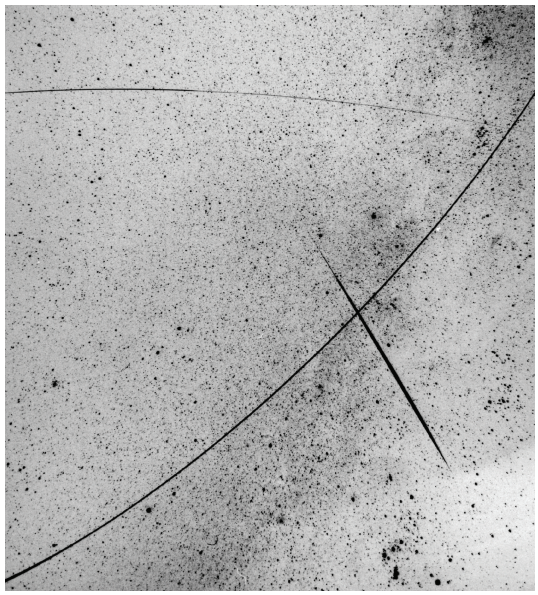

Figure 5: Ondrejov Observatory EN network photographic plate, central part (converted to negative). The EN network uses fish-eye lenses F-Distagon 3.5/30, and the images are recorded on planfilms 90 × 120 mm; sky diamater is 80 mm and typical exposure time 3 hours resulting in limiting magnitude 11.

has two parts, namely, the Peleng 8 mm fish-eye lens (1 : 3,5–1 : 16, Figure 2) that provides a 24 mm circular 180 field of view (Figure 3), and a CANON EOS 350D digital CCD camera (Figure 1). The total cost of the hardware is around 1500 USD, that is, one order less than the CONCAM system. One can hence expect the system to be easily and cheaply replicated to numerous sites. One can consider the alternative type of the digital camera, such as Canon EOS 5D with a larger CCD chip (but somewhat larger pixel size) hence covering the whole FOV of the fish-eye lens. We plan to improve the performance of the system by designing, in collaboration with the Czech Technical University in Prague, especially dedicated mount and miniature dome for the camera. Use of another lens can provide deeper magnitudes but smaller FOV (Figure 8).

Figure 6: The automated EN sky patrol photographic camera operated by the Ondrejov Observatory, Department of Interstellar Matter.

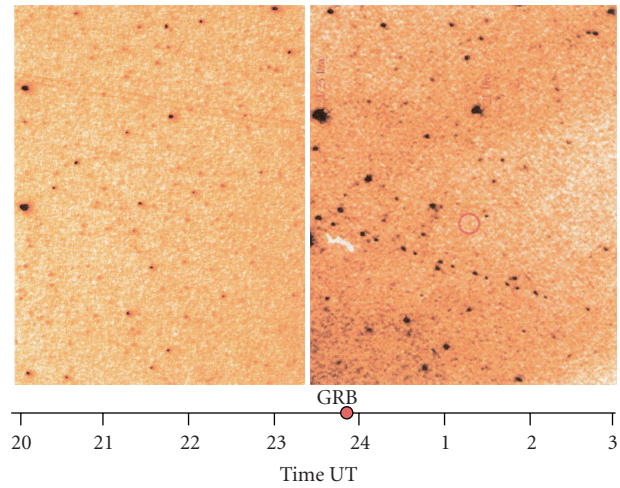

Figure 7: The area of the GRB000926 on the photographic plates of the EN network. Left: preburst image (end of exposure 29 minutes before the GRB trigger), lim magnitude 10. Right: simultaneous image, lim magnitude 8. The position of the GRB is indicated by a circle. Both images contain airplane trails/lights.

3. Simulation and Evaluation of Images from Optical All-Sky Systems

As shown in Figure 2, the all-sky fish-eye lenses consist of 10 glass elements. This type of optics influences the focal images. Any reliable scientific use and evaluation of images from these systems must take this into account. There are two related problems in WFC and UWFC optical systems: (1) optical aberrations, and (2) space variant systems. The motivation for the simulation is as follows:

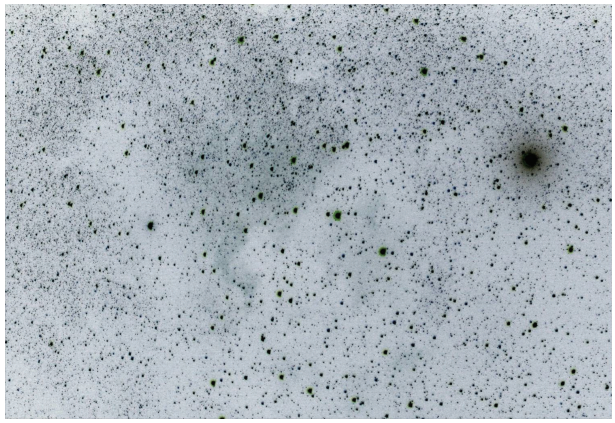

Figure 8: An example of image taken by Canon EOS 350D digital CCD camera with nonfish eye lens Soligor 2.8/105 mm (converted to negative) at Sonneberg Observatory. Then the limiting magnitude amounts to 15 over a smaller FOV of order of 10×10 degrees.

(1) modelling of optical system used in all-sky monitors and their transfer characteristics aberrations and distortion, (2) UPSF image restoration and deconvolution of acquired image data removal, and (3) enhancement of measurement precision.

Real UWFC image data and their evaluation are related with the following problems: (1) objects on ultra-wide-field images are very small (a few pixels per object dimension). (2) Optical aberrations and distortions in UWFC systems, see Figure 11, (3) influence of optical aberrations increases at the edges of FOV and, (4) these aberrations distort the PSF of optical system and rapidly cut the accuracy of measurements. (5) Objects on the frontier of field of view are not used for analysis in astrometry because a lot of aberrations. Above we show several preliminary results obtained in this direction (Figures 9, 10, and 12).

4. The VLF Detections of GRBs

The method of indirect detections of GRBs at Very Low Frequency (VLF) has been described already before [4], however only very few positive records are known. Previously reported VLF detections of GRBs are as follows. (i) GRB830801: a first observation of an ionospheric disturbance from a gamma-ray burst reported [4]. The burst, occurred at 22 : 14 : 18 UT on August 1, 1983, and was one of the strongest ever observed at that time. The total fluency was 0.002 erg/sq cm, most of which occurred in the first 4 seconds of the burst. Simultaneously, a change was observed in the amplitude of a VLF radio signal from a transmitter in Rugby, England indicative of an ionospheric disturbance. Weaker disturbances were also recorded at the same receiving site on signals from VLF stations in Annapolis, Maryland and Lualualei, Hawaii. The times of the burst and the disturbances are coincident within the 10-second resolution of the VLF recording system. No similar disturbances were observed within 60 hours around the time of the burst. (ii) SGR1806: detection of a Sudden Ionospheric Disturbance [5], (iii) GRB030329 observed as a Sudden Ionospheric Disturbance (SID) [6]. Although there were numerous efforts to detect GRBs by VLF and despite the fact that the necessary instrumentation is inexpensive, this field still remains little exploited [7].

The instrumentation used in obtaining the results discussed below consists of a loop radio antenna and a 2-channel VLF radio receiver (Figure 13). The motivation is an alternative and inexpensive approach to detection and investigation of GRBs.

5. Physics of Ionospheric Detection

The solar particle stream, solar wind, shapes and controls the Earths magnetic envelope—the magnetosphere—and increases heat in the aurora zones. But not all ionospheric variability is caused by solar or geomagnetic disturbances. The ionosphere is not a constant "mirror in the sky." The E layer (100–200 km aboveground) and the F1 layer (170–200 km) usually behave in regular, solar-controlled way, but the F2 layer (250–350 km) does not. It is the F2 layer, which has the greatest density of free electrons, and is potentially the most effective reflector of radio waves (see [7]).

The ionospheric D layer plays in the GRB detections an important role, as the detection of X-ray and gamma-ray triggers is based on the measurement (monitoring) of reflected radio waves from this layer. The ionospheric D layer is not transparent for radio VLF waves (frequencies 3 kHz to 30 kHz) and behaves like a mirror. If the transmitter is at large distance (800 to 2000 km) then the radio waves are guided like in a waveguide consisting of the D layer and the earth surface. Any change in the quality of this waveguide results then in the signal change in the SID monitor. The change can be positive but in some cases such as the sudden phase anomaly also negative.

6. VLF Detections of GRBs

We present below examples of our VLF/SID detection of GRBs in three cases: GRB 060124A (Figure 14), GRB080319D and GRB080320A (Figure 15), as well as an indication for detection of GRB induced propagating ionospheric waves (Figure 15).

7. Conclusions

An alternative low-cost (~1.5 kUSD) optical digital all-sky monitoring system has been assembled and it is tested recently. The preliminary results indicate the limiting magnitude even for nonguided system and for one image with exposure of 30 seconds amounts to mag 8. Deeper magnitudes are expected for guided system and longer or cumulated exposures, then the expected limiting magnitude can reach the magnitude 9-10 range. This makes the system suitable for wide-field monitoring in the sky for brighter optical transients. Using nonfish-eye lenses, the limiting

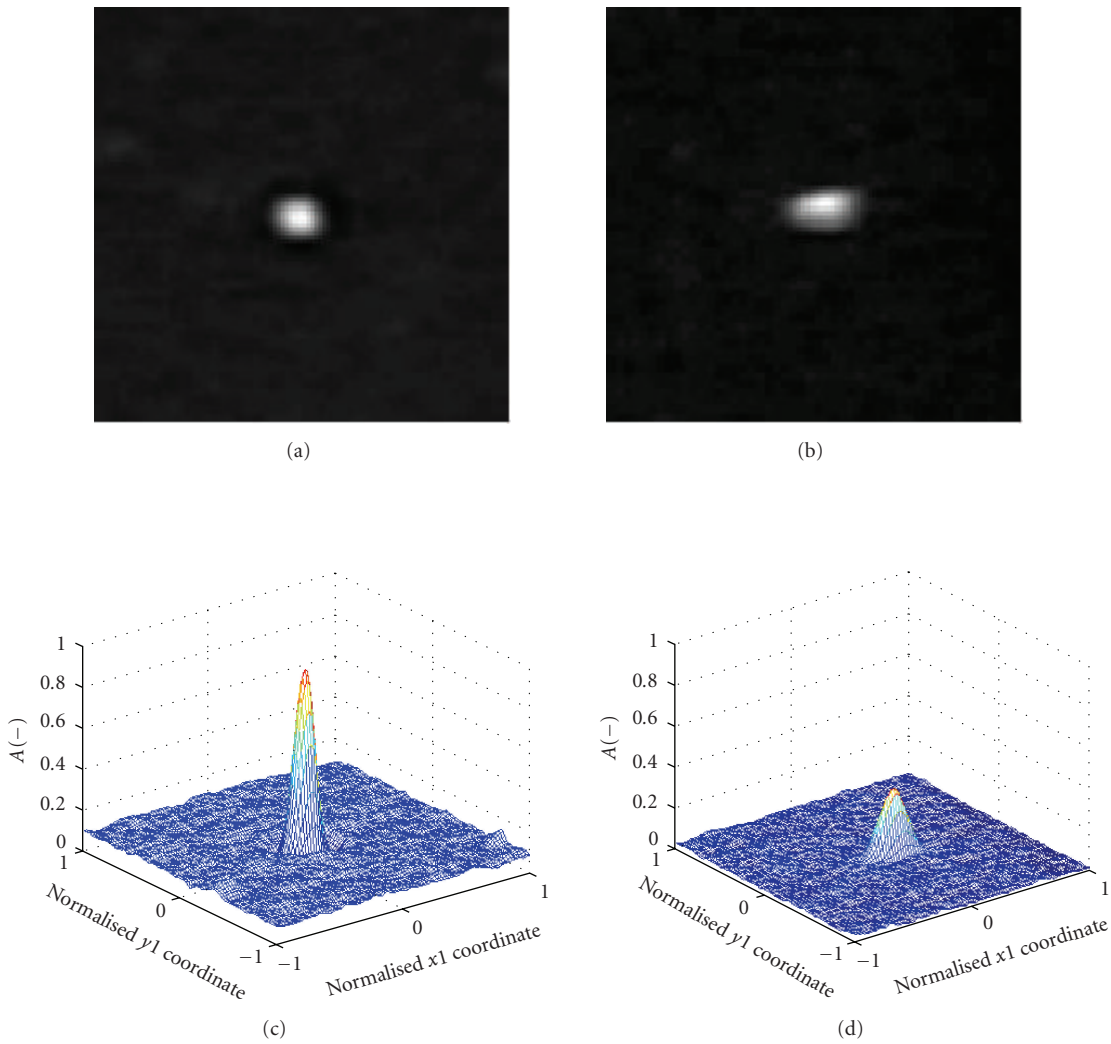

Figure 9: The ellipticity of star profiles (simulation). Profiles of stars also are not circular but rather elliptical, especially for worse objectives and greater distance from the middle of the image. The ellipticity is qualified by sigma x and sigma y (while considering the Gaussian function), where sigma x and sigma y are the distance from the centre of the Gaussian in which the Gaussian is equal to exp(−0,5) of its central value. Sigma x and sigma y are the major and minor half-axis of the ellipse, perpendicular to each other. The ellipticity in radial direction can significantly grow with the angle distance from the middle of the image, especially for wide-angle images.

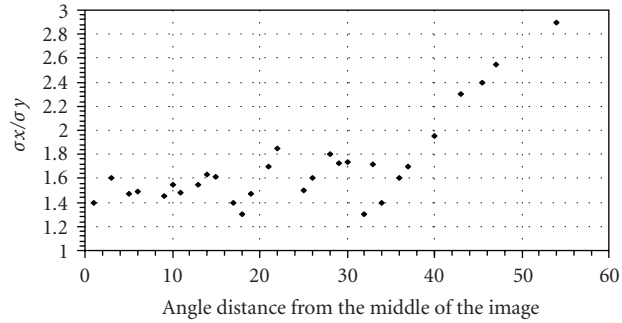

Figure 10: Ellipticity (an ideal PSF deformation) of stars' profiles as a function of angle distance from the middle of an all-sky image.

magnitude can reach 15 over a smaller (10 × 10 degrees) FOV. The system can be very easily duplicated to numerous sites. Future improvements are planned such as design of a miniature camera mount and dome to allow guided images and development of dedicated control and evaluation software. The algorithms for evaluation of images from all-sky monitors were developed and tested.

The independent and indirect detection of GRBs by their ionospheric response (SID) observed at VLF is feasible. We presented and discussed examples of such VLF/SID detection in three cases: GRB 060124A, GRB080319D, and GRB080320A. In addition, these measurements are in agreement with the scenario of propagating ionospheric waves triggered by the relevant GRBs. Although few such detections have been already reported in the past, the capability of such alternative and indirect investigations of GRBs, as well as the possible contribution to analyses of GRBs, still remains to be investigated in more details.

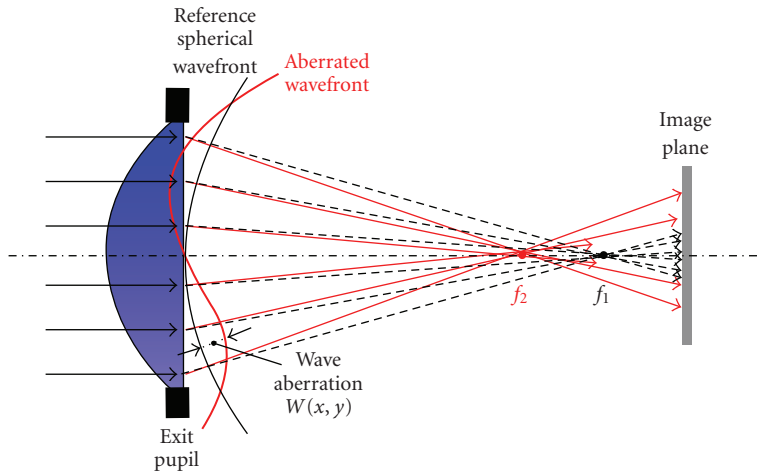

Figure 11: Optical aberration can be described using the so-called wave aberration function. The wave aberration function is defined as the distance (in optical path length) from reference sphere to the wave front in the exit pupil measured along the ray. Optical aberrations negatively affect the image quality, imaging system transfer characteristics, and cut precision of other measurements.

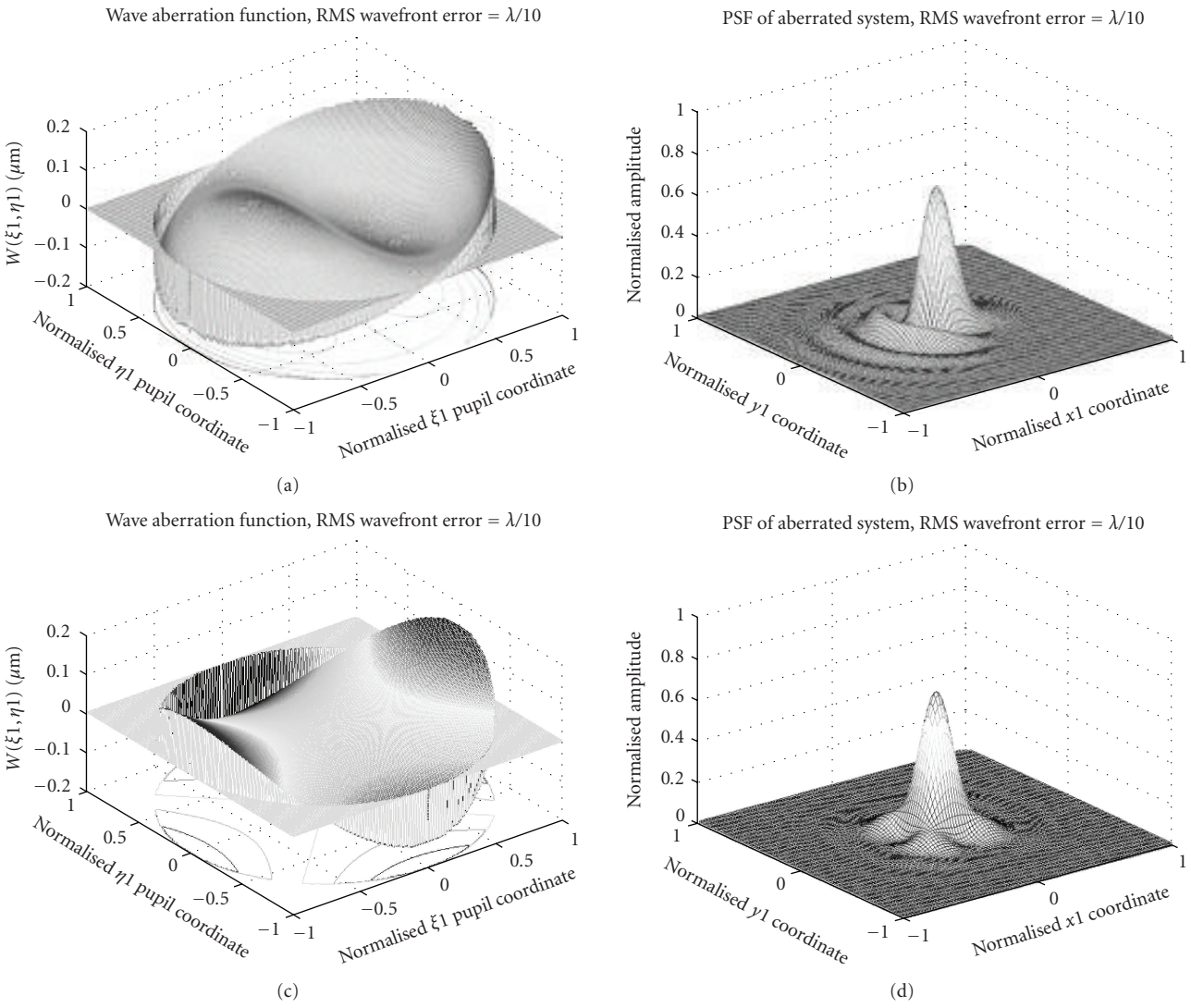

Figure 12: Examples of modelling of optical aberrations in optical all-sky monitors.

(a) (b)

Figure 13: The loop antenna (size 75 × 75 cm) and a 2-channel radio VLF receiver used for SID detection of GRBs.

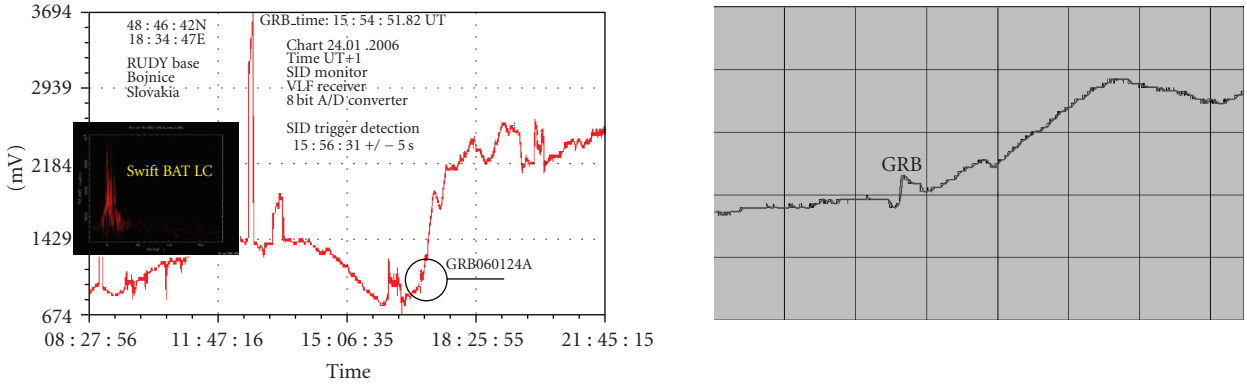

(a) (b)

Figure 14: The detection of GRB 060124A.

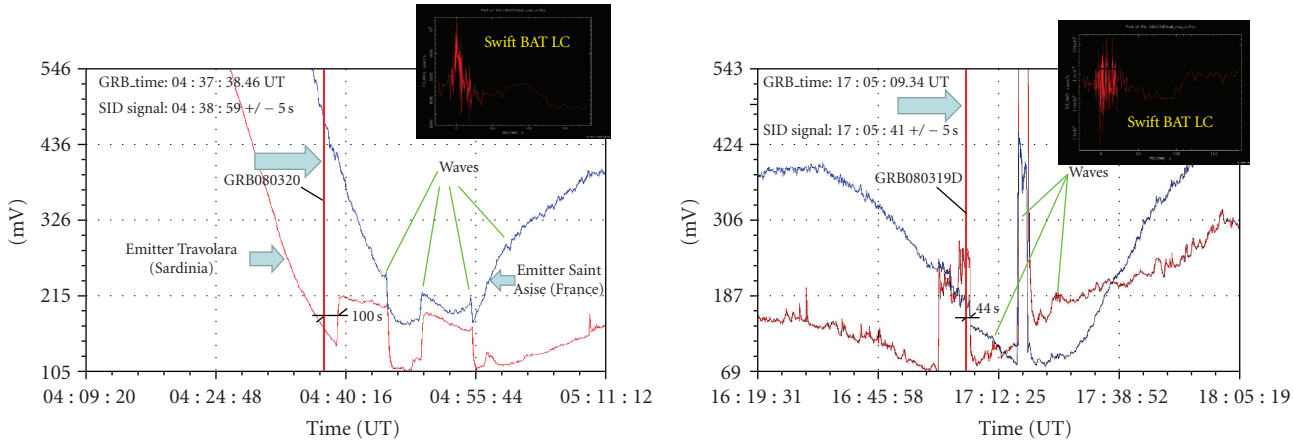

(a) (b)

Figure 15: The probable detection of GRB080319D (a) and GRB080320A (b) with indicated probable propagating ionospheric waves caused by the GRB.

Acknowledgments

The GRB analyses described here are linked to the GRB analyses within the ESA PECS INTEGRAL Project 98023. Some parts are related to the grant of the Grant Agency of the Czech Republic 205/08/1207 and 102/09/0997. The analyses of GRBs in optical range are newly supported by MSMT KONTAKT Project ME09027.

References

[1] C. Akerlof, R. Balsano, S. Barthelmy, et al., "Observation of contemporaneous optical radiation from a γ-ray burst," *Nature*, vol. 398, no. 6726, pp. 400–402, 1999.

[2] J. L. Racusin, S. V. Karpov, M. Sokolowski, et al., "Broadband observations of the naked-eye γ-ray burst GRB 080319B," *Nature*, vol. 455, no. 7210, pp. 183–188, 2008.

[3] M. Jelínek, M. Prouza, P. Kubánek, et al., "The bright optical flash from GRB 060117," *Astronomy and Astrophysics*, vol. 454, no. 3, pp. L119–L122, 2006.

[4] G. J. Fishman and U. S. Inan, "Observation of an ionospheric disturbance caused by a γ-ray burst," *Nature*, vol. 331, no. 6155, pp. 418–420, 1988.

[5] P. Campbell, M. Hill, R. Howe, et al., "SGR1806: detection of a sudden ionospheric disturbance," GCN GRB Observation Report 2932, GRB Coordinates Network, AAVSO, Cambridge, Mass, USA, 2003.

[6] P. W. Schnoor, D. L. Welch, G. J. Fishman, and A. Price, "GRB030329 observed as a sudden ionospheric disturbance (SID)," GCN GRB Observation Report 2176, GRB Coordinates Network, AAVSO, Cambridge, Mass, USA, 2003.

[7] H. Rishbeth, I. C. F. Müller-Wodarg, L. Zou, et al., "Annual and semiannual variations in the ionospheric F2-layer. II. Physical discussion," *Annales Geophysicae*, vol. 18, no. 8, pp. 945–956, 2000.